JOURNAL OF ENVIRONMENTAL SCIENCES 67 (2018) 171–178

Available online at www.sciencedirect.com

ScienceDirect

www.elsevier.com/locate/jes

JES JOURNAL OF ENVIRONMENTAL SCIENCES

www.jesc.ac.cn

Adsorption of VOCs on reduced graphene oxide

Lian Yu[1,*], *Long Wang*[1], *Weicheng Xu*[1], *Limin Chen*[1,2,3], *Mingli Fu*[1,2,3], *Junliang Wu*[1,2,3], *Daiqi Ye*[1,2,3,*]

1. *College of Environment and Energy, South China University of Technology, Guangzhou 510006, China*
2. *Guangdong Provincial Key Laboratory of Atmospheric Environment and Pollution Control, Guangzhou 510006, China*
3. *National Engineering Laboratory for VOCs Pollution Control Technology and Equipment, South China University of Technology, Guangzhou 510006, China*

ARTICLE INFO

Article history:
Received 31 March 2017
Revised 23 August 2017
Accepted 28 August 2017
Available online 8 September 2017

Keywords:
Graphene oxide
Reduced graphene oxide
Volatile organic compounds
Adsorption

ABSTRACT

A modified Hummer's method was adopted for the synthesis of graphene oxide (GO) and reduced graphene oxide (rGO). It was revealed that the modified method is effective for the production of GO and rGO from graphite. Transmission electron microscopy (TEM) images of GO and rGO showed a sheet-like morphology. Because of the presence of oxygenated functional groups on the carbon surface, the interlayer spacing of the prepared GO was higher than that of rGO. The presence of –OH and C═O groups in the Fourier transform infrared spectra (FTIR) spectrum and G-mode and 2D-mode in Raman spectra confirmed the synthesis of GO and rGO. rGO (292.6 m^2/g) showed higher surface area than that of GO (236.4 m^2/g). The prepared rGO was used as an adsorbent for benzene and toluene (model pollutants of volatile organic compounds (VOCs)) under dynamic adsorption/desorption conditions. rGO showed higher adsorption capacity and breakthrough times than GO. The adsorption capacity of rGO for benzene and toluene was 276.4 and 304.4 mg/g, respectively. Desorption experiments showed that the spent rGO can be successfully regenerated by heating at 150.0°C. Its excellent adsorption/desorption performance for benzene and toluene makes rGO a potential adsorbent for VOC adsorption.

Introduction

Volatile organic compounds (VOCs) include aromatic, aliphatic and chlorinated hydrocarbons *etc.*, which are emitted into the atmosphere mainly from human activities, such as production of adhesives, paints, printing materials, building materials and chemicals for synthesis (Li et al., 2010; Sakai et al., 2017). In recent years, VOCs have become one of the most harmful types of pollutants toward human health, which can cause a series of symptoms such as nausea, headache, coryza, pharyngitis, emphysema, lung cancer, and even death (Yi et al., 2009; Dai et al., 2017). Since the presence of VOCs in the atmosphere can cause severe health problems, they have attracted extensive attention, and many efforts have been dedicated to the removal of VOCs in recent years. Several physical–chemical technologies including adsorption (Jia et al., 2017), condensation (Hamad and Fayed, 2004), incineration (Campesi et al., 2015), catalytic combustion (Wang et al., 2017) and thermal oxidation (Mao et al., 2015) have been used to remove VOCs from gaseous streams. Among these methods, the adsorption technique has been widely used due to its low cost and easy application at large scale.

As adsorbents, carbon-based materials such as activated carbon (Li et al., 2016a), graphene (Wang et al., 2015), carbon nanotubes (Li et al., 2016b) and porous carbon (Qi et al., 2017), have attracted much attention. Due to their unique structure

* *Corresponding authors. E-mails:* esyulian@scut.edu.cn (Lian Yu), cedqye@scut.edu.cn (Daiqi Ye).

http://dx.doi.org/10.1016/j.jes.2017.08.022

and large surface area, graphene-based materials have been used as superior adsorbents for the removal of toxic pollutants from the natural environment (Yu et al., 2016). Graphene is extremely hydrophobic and its theoretical specific surface area is as high as 2600 m^2/g (Zhao et al., 2014); it is expected to possess excellent adsorption capacity for hydrophobic organic compounds and can be used as an excellent adsorbent in air purification. Graphene oxide (GO) is a graphene sheet, with carboxylic groups at its edges and epoxide groups and phenolic hydroxyl on its basal plane. Chemical treatment or thermal annealing can eliminate the functional groups on GO, which can produce reduced graphene oxide (rGO) (Yu et al., 2016). Compared with GO, rGO shows better adsorption performance for aromatic pollutants due to its lower oxygen content, higher hydrophobicity and higher surface area. Chen and Chen (2015) studied the adsorption of m-dinitrobenzene, nitrobenzene, and *p*-nitrotoluene onto GO and rGO. They found that rGO nanosheets, which had more defect sites than GO, exhibited higher adsorption capacity for nitroaromatic compounds, which was 10–50 times higher than the reported adsorption by carbon nanotubes. It has been demonstrated that in addition to the hydrophobic effect, π–π interactions were also responsible for the strong adsorption of organic molecules onto graphene materials (Wang et al., 2014). Wang et al. (2015) studied the adsorption of phenolic compounds onto rGO and found that the adsorption was dependent on π–π interactions between the aromatic molecules and rGO; both the chemical structure of the phenolics and the degree of reduction of rGO can influence the π–π interactions. Because of the π–π interaction, rGO shows strong adsorption ability for chemicals with one or more benzene rings. Nevertheless, as far as we know, the adsorption of VOCs by rGO has not been paid much attention.

In this work, we report a cost-effective and facile method to prepare rGO, derived from few-layered graphite oxide. The microstructure and surface characteristics of rGO were studied using transmission electron microscopy (TEM), X-ray diffraction (XRD), Raman spectroscopy, Fourier transform infrared spectra (FTIR) and N_2 adsorption and desorption isotherms. The prepared rGO was used as an adsorbent for benzene and toluene, model pollutants of VOCs, and its adsorption performance was compared with that of GO. The relatively longer breakthrough time and gradual increase of VOC concentration following breakthrough observed for this material are promising features. The regeneration of saturated rGO is another critical factor that should be considered while selecting an adsorbent. Therefore, dynamic adsorption/desorption experiments to study the adsorption performance of rGO were also carried out.

1. Experiment

1.1. Chemicals

rGO was prepared by reducing GO according to a method reported previously (Yu et al., 2016). Graphite flake with an average diameter of 20 μm (99.95 wt.% purity) was obtained from Yingshida graphite Co. Ltd., Qingdao, China. Sulfuric acid (H_2SO_4, 98.0 wt.%), hydrogen peroxide (H_2O_2, 30.0 wt.%), potassium permanganate ($KMnO_4$), sodium nitrate ($NaNO_3$), hydrochloric acid (HCl), hydrazine hydrate (H_6N_2O), benzene, and toluene were of analytical grade and purchased from Sinopharm Chemical Reagent Co., Ltd. All chemicals were used without further purification. Ultrapure water (18.0 MΩ·cm) used in all experiments was produced using a Millipore-ELIX water purification system.

1.2. Materials synthesis

1.2.1. Preparation of GO

GO was synthesized using a modified Hummer's method (Rajaura et al., 2016). The starting material for preparation of GO was graphite powder, $KMnO_4$, $NaNO_3$, H_2O_2, and concentrated H_2SO_4. Graphite powder (3.0 g) and $NaNO_3$ (2.0 g) were stirred in 70.0 mL of concentrated H_2SO_4 at a temperature of 0°C. Then, $KMnO_4$ (9.0 g) was slowly added into the mixture and the temperature was kept below 20.0°C. Then, the ice bath was removed from the reaction flask, the mixture in flask warmed up to room temperature, and again the mixture was stirred for 15.0 min. After that, deionized water (250.0 mL) was slowly added to the mixture and stirred for 15.0 min; during this process, the temperature of the mixed solution was kept below 100.0°C. Then, 30.0% H_2O_2 was added to the solution followed by stirring for 24.0 hr. Finally, the mixture was centrifuged at 7000 rotations per minute (r/min) using a rotary centrifuge. The brown pasty material obtained was GO.

1.2.2. Preparation of rGO

The prepared GO was dispersed in distilled water under continuous stirring at a temperature of 35.0°C to prepare colloidal GO. A solution of hydrazinium hydroxide (H_6N_2O, as a reducing agent) was then added in the above colloid, which was then stirred at 60.0°C for 3.0 hr. Then, the mixture turned from brown to black and was filtered to obtain black powdered rGO (Rajaura et al., 2016). The prepared samples were freeze-dried under vacuum for 24.0 hr.

1.3. Characterization techniques

The structural and morphological properties of rGO were characterized using various analytic and spectroscopic techniques. Transmission electron microscopy (TEM) observations were carried out by using a Tecnai G^2 20 S-TWIN microscope (Tecnai G^2 F20 S-TWIN, FEI, USA) with an accelerating voltage of 200 kV. X-ray diffraction (XRD) patterns of the samples were measured from 5° to 60° using a Philips X'Pert PRO (X'Pert PRO, Panalytical, Netherlands) X-ray diffraction instrument. Raman spectra were recorded with a Renishaw INVIA Raman spectrometer (INVIA, Renishaw plc, UK). Fourier transform infrared spectra (FTIR) were recorded on a Shimadzu IR Prestige-21 FTIR spectrophotometer (Prestige-21, Shimadzu, Japan) in the range of 4000–400 cm^{-1} using the KBr disc technique. N_2 sorption isotherms were recorded with a Micromeritics TriStar II 3020 surface area and porosity analyzer (TriStar II 3020, Micromeritics Instrument Corporation, USA). Before measurement, the as-prepared samples were degassed under vacuum at 120.0°C for 12.0 hr. The specific surface area results were calculated using the BET (Brunauer–Emmett–Teller) method based on the adsorption data. The pore size distribution was determined via the BJH (Barrett–Joyner–Halenda) method using nitrogen adsorption data.

1.4. Adsorption measurements

The cyclic adsorption/desorption experiments of benzene and toluene on GO and rGO were carried out in a continuous flow tube reactor made of iron. The parameters such as bed depth and flow rate were fixed at 10.0 cm and 40.0 mL/min, respectively. The 1, 2, 3 and 4 in the diagram are valves. The reactor was placed in a programmable furnace, so that the temperature inside the reactor could be regulated. In the adsorption experiment, GO or rGO (500.0 mg) was loaded in a tube reactor, and a 40.0 mL/min N_2 flow containing 50.0 ppm benzene (toluene) vapor was then passed through the tube reactor until adsorption equilibrium. Gaseous benzene and toluene were prepared by bubbling N_2 into liquid benzene and toluene that were kept at 10.0°C with a thermostatic water bath. Then, benzene or toluene was mixed with diluent gas (N_2) in a gas-mixing chamber to acquire the desired concentration. A flowmeter was applied to adjust the flow rate of VOCs, in order to maintain the concentration of benzene and toluene at a constant level. In order to obtain the breakthrough curve of the dynamic adsorption experiment, the gas concentration at the inlet and outlet of the reactor was detected by a gas chromatograph (GC) (7890A, Agilent, USA) equipped with a hydrogen flame ionization detector (FID). The time when the outlet concentration of VOCs is 5.0% of the inlet concentration was defined as the breakthrough time. The adsorption capacity for the VOCs was calculated by numerical integration of the breakthrough curve. After saturation of the adsorbent bed, desorption experiments were carried out using the same experimental setup as adsorption (Fig. 1). The desorption experiments were carried out in a N_2 flow (30.0 mL/min) at a heating rate of 10.0°C/min up to 150.0°C, and the temperature of the outlet gas was detected by a resistance thermometer sensor.

2. Results and discussion

2.1. Characterization of the as-synthesized materials

The TEM images of GO and rGO are presented in Fig. 2a and b. The nature of graphene can be identified by the typical ripples present on the GO and rGO surfaces (Wang et al., 2014). As can be seen from Fig. 2, there are many wrinkles located at the edge of GO, GO nanosheets are slightly aggregated, and the surface of rGO is relatively flat compared with that of GO. In Fig. 2b, rGO presents a large, entangled and almost transparent morphology, where the nearly invisible areas are due to the ultrathin character of the rGO nanosheets. As VOC molecules were mainly adsorbed onto the surface of rGO (GO), the flat surfaces and wrinkled regions are both potential adsorption sites; as rGO nanosheets are dispersed better than GO, rGO may be expected to show higher adsorption capacity than that of GO.

Fig. 3 shows XRD patterns of GO, rGO and rGO treated at 150°C. The interlayer distance of GO calculated from the (001) plane at $2\theta = 11.4°$ was 0.78 nm, which is much larger than that of pristine graphite (~0.34 nm); this can be attributed to the introduction of a large number of oxygenated functional groups (such as epoxy, carbonyl, hydroxyl and carboxyl) into the graphite layers during the process of oxidation (Sui et al., 2014). As the inter-layer space in the graphite layer increased, the surface area of GO and rGO increased, which is favorable for VOC adsorption. After hydrothermal reduction, the peak at $2\theta = 11.4°$ completely disappeared, and a broad peak centered at around $2\theta = 25.2°$ (d_{002} of *ca*. 0.37 nm) was observed for the rGO, confirming the reduction of GO and the recovery of the graphitic structure (Sui et al., 2014); rGO also exhibits a peak at 44.5°, which can be attributed to the (100) plane (Jiang et al.,

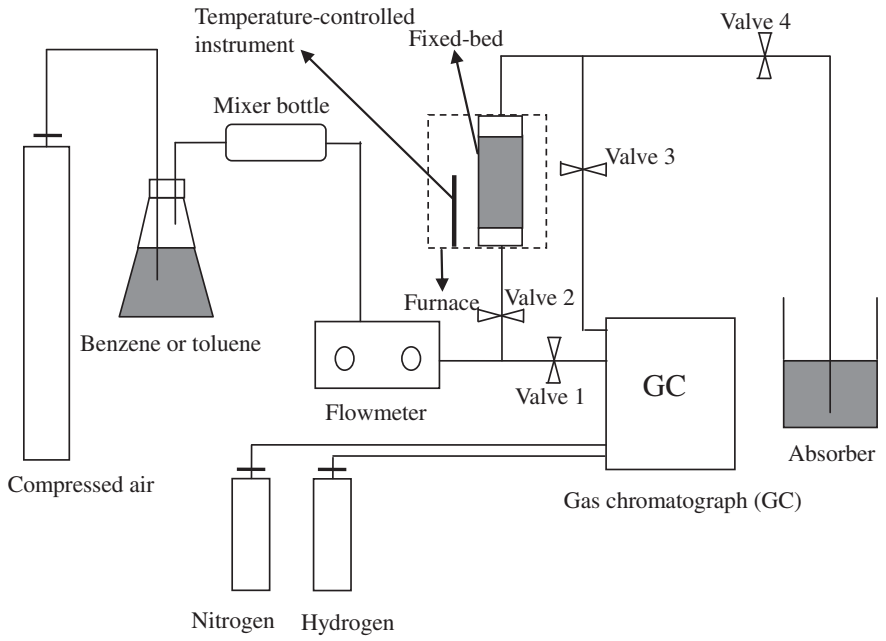

Fig. 1 – Schematic diagram of the experimental setup.

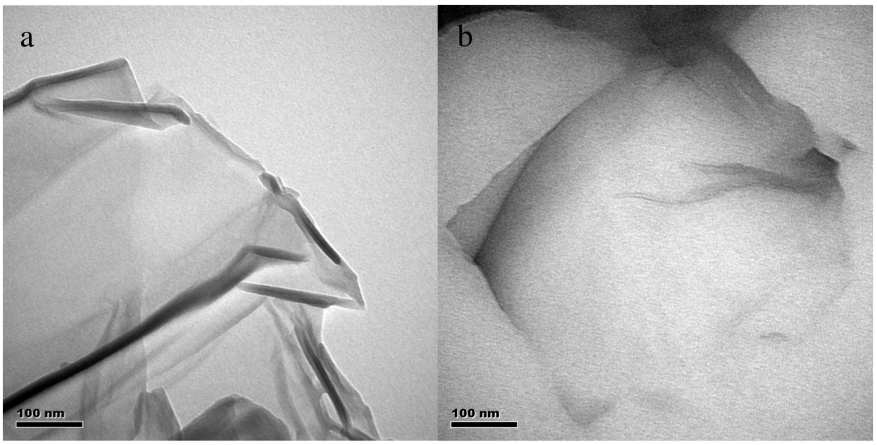

Fig. 2 – Transmission electron microscopy (TEM) images of the as-synthesized graphene oxide (GO) (a) and reduced graphene oxide (rGO) (b).

2016). As can be seen from Fig. 3, the intensities for the (002) and (100) reflections of rGO treated at 150°C were a little lower than those of rGO, but the XRD patterns of rGO and rGO treated at 150°C were almost the same, indicating the thermal stability of rGO.

Raman spectroscopy can be used to characterize the sp^2 and sp^3 hybridization of carbon atoms in graphite, GO and rGO. Single, double, and multi-layer graphene can be differentiated by their Raman fingerprints (Rajaura et al., 2016). The Raman spectra of GO and rGO are shown in Fig. 4. As can be seen, the D and G bands of GO observed at wave numbers 1362.5 and 1589.6 cm^{-1} are shifted to 1348.2 and 1577.2 cm^{-1} in the case of rGO. The G-band arises from the stretching of the C-C bond in graphitic materials, which is typical of all sp^2 carbon systems. The D-mode originates from defects, disordered sp^2-hybridization, and some impurity structure of GO. The relative intensity ratio of the D and G bands of GO is about 0.68, while in the case of rGO, the value is about 0.81. The higher value of the intensity ratio for rGO suggests the presence of defects that remained even after the removal of a large amount of oxygen-containing functional groups (Rajaura et al., 2016). This further confirms that GO is reduced to rGO. The presence of the 2D band in GO located at 2698.6 cm^{-1} can be attributed to a second-order two-phonon Raman process. The 2D band in GO suggests that all of the graphite layers have been oxidized, which is consistent with the XRD results in Fig. 3. The absence of the 2D band in the Raman spectra of rGO indicates the removal of oxygenated functional groups in GO by chemical reduction (Rajaura et al., 2016).

FTIR spectroscopy was used to confirm the process of the preparation of GO and rGO. As can be seen in Fig. 5, the peak located at 3432.8 cm^{-1} is attributed to the bending and stretching of the widespread O–H groups on GO and rGO. The peak located at 2368.3 cm^{-1} is related to the stretching of sp^2 and sp^3 hybridized C–H bonds present in graphite (Rathnayake et al., 2017). Two weak peaks at 1643.1 and 1577.6 cm^{-1} are related to the C=O stretching vibration (indicating the presence of carboxylic acid or carbonyl groups) and C–C (in–ring) stretching vibrations (indicating the presence of non-oxidized carbon rings; as for rGO, it has two resonance structures: diene and dienophile). The peaks at 1438.7 and 674.9 cm^{-1} can be attributed to the

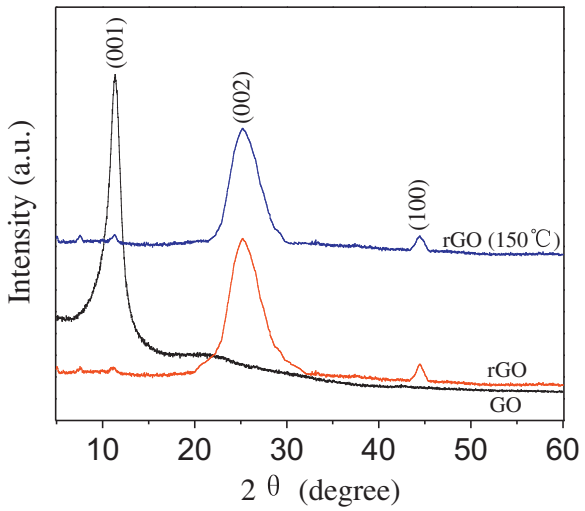

Fig. 3 – X-ray diffractograms obtained on GO, rGO and rGO treated at 150°C.

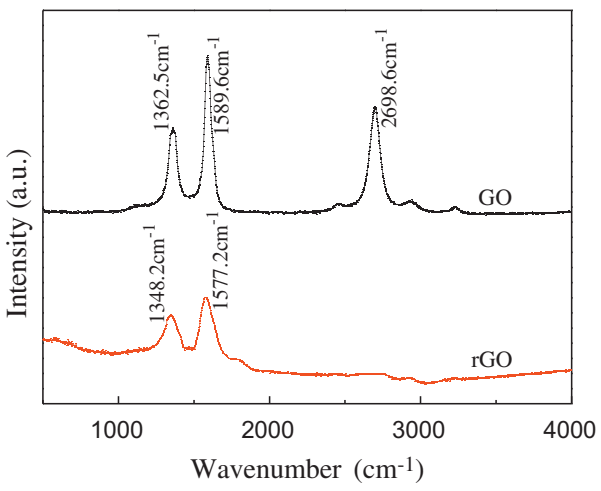

Fig. 4 – Raman spectra of GO and rGO.

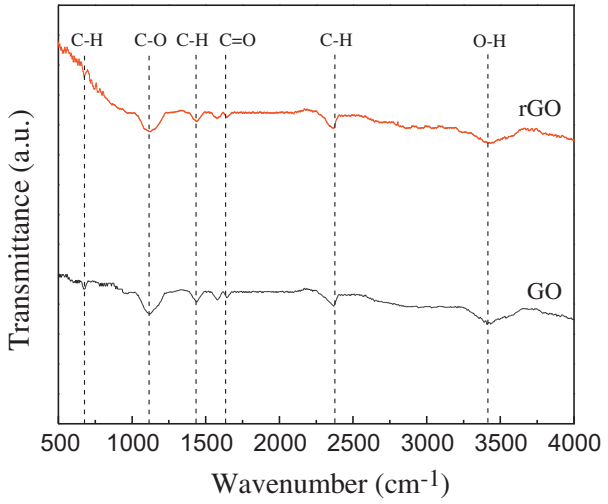

Fig. 5 – FTIR (Fourier transform infrared spectra) spectra of GO and rGO.

bending of aromatic C–H bonds. The peak at 1122.4 cm^{-1} corresponds to C–O bonds (epoxy or alkoxy). It also can be found that the intensities of C═O, O–H and C–O peaks in rGO are lower in comparison to GO.

The specific textural properties of GO and rGO were analyzed by N_2 adsorption–desorption measurements. The N_2 adsorption–desorption isotherms and the corresponding pore size distribution curves of GO and rGO are shown in Fig. 6. Both of the isotherms exhibit N_2 adsorption isotherms of type IV, which indicates the presence of mesopores. The isotherm of GO is below the isotherm of rGO; this can be due to the filling of the interlayer space with various functional groups for GO (Ganesan and Shaijumon, 2016). The BJH pore size distribution (Fig. 6b) revealed the pore diameters in GO and rGO; the peaks in the distribution for GO and rGO are mainly located around 3.8–4.8 and 4.6–6.2 nm, respectively. Compared with GO (BET surface area, 236.4 m^2/g), rGO has a higher BET surface area (292.6 m^2/g), which is higher than that reported for rGO (surface area, 209.0 m^2/g) by Nawaz et al. (2017), and the higher surface area is beneficial for the adsorption of more pollutants. The higher surface area directly reflects the higher exfoliation degree of graphene materials, as compared with graphite (4.5 m^2/g) (Wang et al., 2014). However, the surface areas of the obtained GO and rGO are lower than the theoretical value (~2630 m^2/g); this should be attributed to the occurrence of incomplete exfoliation and aggregation during the sample preparation process.

2.2. Dynamic adsorption and desorption studies

The prepared rGO was utilized as an adsorbent for the removal of VOCs. For comparison purposes, GO was also tested. The dynamic adsorption experiments were conducted in a continuous flow reactor; Fig. 7a and b show the breakthrough curves for benzene and toluene adsorption on GO and rGO at room temperature. The adsorption capacity was calculated based on the breakthrough curves. In the first run, the adsorption capacity for benzene was 276.4 mg/g (rGO) and 216.2 mg/g (GO), respectively. As for toluene, the adsorption capacity was 304.4 mg/g (rGO) and 240.6 mg/g (GO), respectively. It can be seen that the adsorption capacity of toluene is higher than that of benzene both for rGO and GO. It is well-known that both the surface chemistry and the micro-structure of rGO are important factors determining the adsorption of different VOCs (Lemus et al., 2012). Increasing the surface area of sorbents can generally improve the adsorption performance, but the chemical functional groups at the surface of the sorbents play an important role in benzene and toluene adsorption. In the processes of benzene and toluene adsorption, different mechanisms may act simultaneously; mainly, electrostatic interactions, π–π bonds and hydrophobic interactions. Due to the presence of benzene rings and the hydrophobic surface, electrostatic interactions, π–π bonds and hydrophobic interactions between the aromatic compounds and rGO are expected. There is one benzene ring in the molecular structure of both benzene and toluene, and the only difference is that toluene has an extra methyl group in its structure. The methyl group of toluene can interact with the O-containing groups at the surface of rGO via hydrogen bonding, which can enhance the interaction between toluene and rGO.

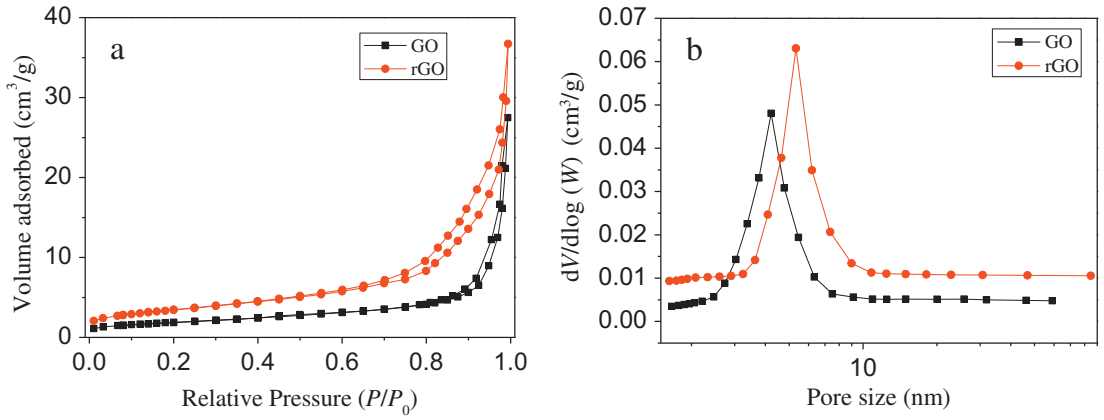

Fig. 6 – (a) Nitrogen adsorption–desorption isotherms and (b) BJH (Barrett–Joyner–Halenda) pore size distribution curves of GO and rGO. *P*: the gas phase pressure when adsorption equilibrium achieved; P_0: the saturated vapor pressure; *V*: volume; *W*: width.

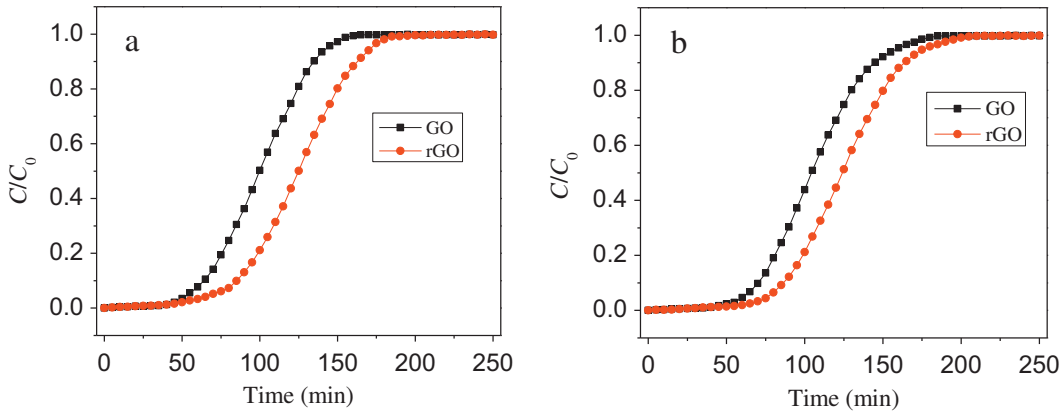

Fig. 7 – Breakthrough curves of benzene (a) and toluene (b) on GO and rGO obtained at room temperature. C_0: the initial concentration; C: the concentration at time t.

For an excellent adsorbent, the ability to keep its adsorption capacity after successive adsorption/desorption cycles is very important. As can be seen from Fig. 1, the regeneration (desorption) of saturated rGO was conducted by heating the tube reactor with a furnace. As can be seen from Fig. 8a, the breakthrough point of the second run was markedly earlier compared with the first run. The breakthrough curves in the last three runs were quite similar, suggesting that the adsorption behaviors were reproduced in the successive adsorption/desorption processes; whereas, as can be seen from Fig. 8b, the desorption profiles seem a little different from each other in the four runs. It was difficult to conduct a manual sampling to conduct at the same time point in the four desorption runs. Therefore, the obtained desorption profiles could not accurately reflect the real-time changes of concentration of the outlet gas. In any case, the desorption curves reflected the fact that most of the toluene was desorbed within 30.0 min in each desorption run, and the concentration of toluene in the outlet gas could reach up to 1600.0 ppm, indicating that toluene was quickly desorbed from rGO and well-concentrated. The outlet concentration dropped to below 2.0 ppm within 50.0 min, and the adsorption capacity in the successive adsorption/desorption runs remained almost unchanged, suggesting that rGO can be effectively regenerated by thermal desorption. Furthermore, temperature monitoring showed that the temperature of the outlet gas was generally lower than 40.0°C in the first 20.0 min during the thermal desorption process, which was beneficial to the recycling of the VOCs by freezing condensation.

Fig. 9 shows the breakthrough curves of toluene adsorption on rGO and GO under humid conditions in the presence of 300.0 ppm water vapor, and the other experimental conditions were the same as under dry conditions. The breakthrough curves for dry and humid conditions were similar, and the calculated adsorption capacity of rGO was 304.4 and 243.8 mg/g, respectively. This indicated that approximately 80.1% of the adsorption capacity of rGO was still retained under the condition of high humidity; the decrease of the adsorption capacity could be due to competitive adsorption with water vapor. The initial concentrations for toluene and water vapor were 50.0 and 300.0 ppm, respectively, but the adsorption capacity for toluene remained relatively high. As for GO, the calculated adsorption capacity under dry and humid conditions was 240.6 and 79.9 mg/g, respectively, showing that the adsorption capacity of GO decreased significantly compared to that of rGO under humid conditions, suggesting that rGO is rather water-resistant. It has been reported that the graphitized structure can ensure high hydrophobicity (Du and Miller, 2007), and this is a desirable feature for applications in humid conditions.

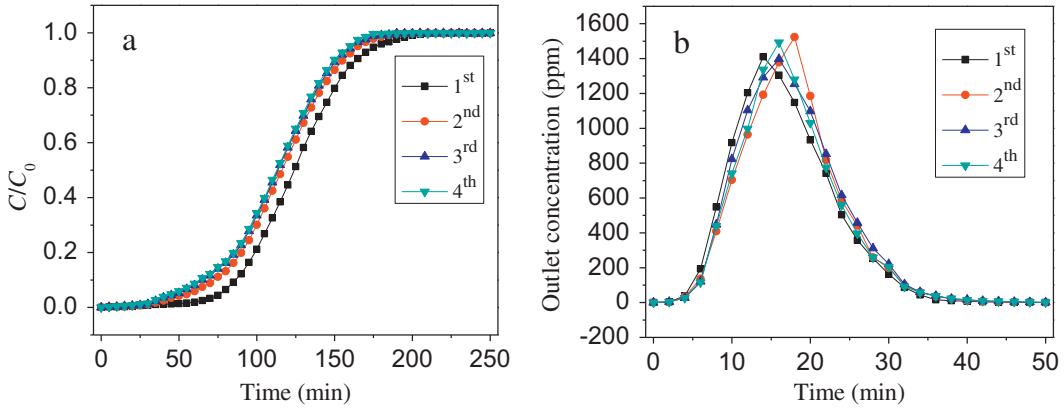

Fig. 8 – Cyclic adsorption/desorption profiles of toluene on rGO: (a) the breakthrough curves obtained at room temperature and (b) the thermal desorption curves obtained at 150.0°C.

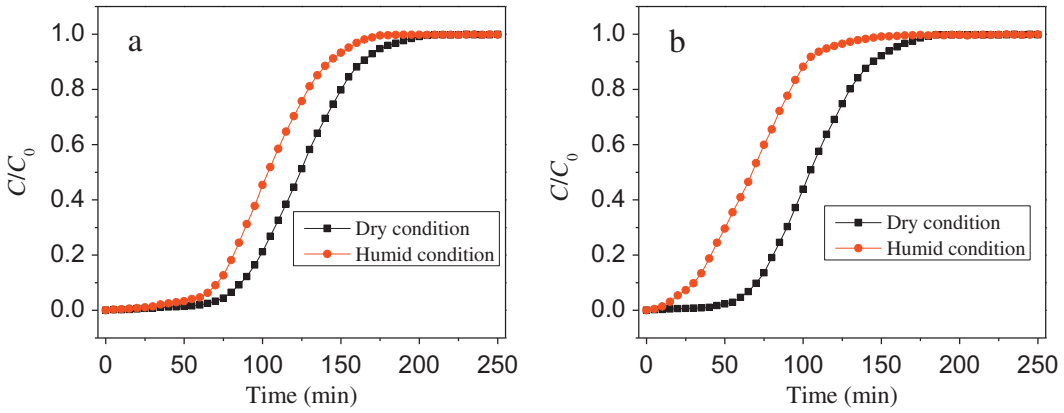

Fig. 9 – Breakthrough curves for toluene adsorption on rGO (a) and GO (b) in the presence of 300.0 ppm water vapor at room temperature.

3. Conclusion

This study presented the preparation of rGO with high purity and crystallinity by a modified Hummer's method. GO and rGO showed a packed sheet-like morphology. The interlayer spacing of the prepared GO was relatively large, likely due to the introduction of oxygenated functional groups to the carbon surface; after hydrothermal reduction, the interlayer spacing of rGO decreased, indicating the recovery of the graphitic structure. The BET surface areas of GO and rGO were 236.4 and 292.6 m^2/g, respectively. The adsorption experiment results show that rGO possessed a higher benzene and toluene adsorption capacity than GO, and the breakthrough adsorption capacity of rGO for benzene and toluene at normal pressure and room temperature was 276.4 and 304.4 mg/g, respectively. Desorption experiments showed that the regeneration of the spent rGO could be successfully realized by heating at 150.0°C. rGO shows potential as an adsorbent for adsorption of VOCs (at ppm levels) under dynamic adsorption/desorption conditions.

Acknowledgments

This work is financially supported by the China Postdoctoral Science Foundation (2016M592496), National Natural Science Foundation of China (Nos. 91645119, 21207039, U1201231, 51378218, 51108187 and 50978103), the Fundamental Research Funds for the Central Universities (Nos. 2017BQ053 and 2017BQ055), Natural Science Foundation of Guangdong Province, China (Grant No. 2014A030310431) and Guangzhou Science and Technology Plan (201607010095).

REFERENCES

Campesi, M.A., Luzi, C.D., Barreto, G.F., Martínez, O.M., 2015. Evaluation of an adsorption system to concentrate VOC in air streams prior to catalytic incineration. J. Environ. Manag. 154, 216–224.

Chen, X.X., Chen, B.L., 2015. Macroscopic and spectroscopic investigations of the adsorption of nitroaromatic compounds on graphene oxide, reduced graphene oxide, and graphene nanosheets. Environ. Sci. Technol. 49, 6181–6189.

Dai, H.X., Jing, S.G., Wang, H.L., Ma, Y.G., Li, L., Song, W.M., et al., 2017. VOC characteristics and inhalation health risks in newly renovated residences in Shanghai, China. Sci. Total Environ. 577, 73–83.

Du, H., Miller, J.D., 2007. Adsorption states of amphipatic solutes at the surface of naturally hydrophobic minerals: a molecular dynamics simulation study. Langmuir 23, 11587–11596.

Ganesan, A., Shaijumon, M.M., 2016. Activated graphene-derived porous carbon with exceptional gas adsorption properties. Microporous Mesoporous Mater. 220, 21–27.

Hamad, A., Fayed, M.E., 2004. Simulation-aided optimization of volatile organic compounds recovery using condensation. Chem. Eng. Res. Des. 82, 895–906.

Jia, L.J., Ma, J.K., Shi, Q.Y., Long, C., 2017. Prediction of adsorption equilibrium of VOCs onto hyper-cross-linked polymeric resin at environmentally relevant temperatures and concentrations using inverse gas chromatography. Environ. Sci. Technol. 51, 522–530.

Jiang, T.T., Li, J.L., Sun, Z., Liu, X.J., Lu, T., Pan, L.K., 2016. Reduced graphene oxide as co-catalyst for enhanced visible light photocatalytic activity of BiOBr. Ceram. Int. 42, 16463–16468.

Lemus, J., Martin-Martinez, M., Palomar, J., Gomez-Sainero, L., Gilarranz, M.A., Rodriguez, J.J., 2012. Removal of chlorinated organic volatile compounds by gas phase adsorption with activated carbon. Chem. Eng. J. 211–212, 246–254.

Li, S.D., Tian, S.H., Du, C.M., He, C., Cen, C.P., Xiong, Y., 2010. Vaseline-loaded expanded graphite as a new adsorbent for toluene. Chem. Eng. J. 162, 546–551.

Li, J.G., Zhang, P.Y., Wang, J.L., Wang, M.X., 2016a. Birnessite-type manganese oxide on granular activated carbon for formaldehyde removal at room temperature. J. Phys. Chem. C 120, 24121–24129.

Li, M.S., Wu, S.C., Shih, Y.H., 2016b. Characterization of volatile organic compound adsorption on multiwall carbon nanotubes under different levels of relative humidity using linear solvation energy relationship. J. Hazard. Mater. 315, 35–41.

Mao, M.Y., Li, Y.Z., Hou, J.T., Zeng, M., Zhao, X.J., 2015. Extremely efficient full solar spectrum light driven thermocatalytic activity for the oxidation of VOCs on OMS-2 nanorod catalyst. Appl. Catal. B Environ. 174–175, 496–503.

Nawaz, M., Miran, W., Jang, J., Lee, D.S., 2017. One-step hydrothermal synthesis of porous 3D reduced grapheme oxide/TiO_2 aerogel for carbamazepine photodegradation in aqueous solution. Appl. Catal. B Environ. 203, 85–95.

Qi, J.W., Li, J.S., Li, Y., Fang, X.F., Sun, X.Y., Shen, J.Y., et al., 2017. Synthesis of porous carbon beads with controllable pore

structure for volatile organic compounds removal. Chem. Eng. J. 307, 989–998.
Rajaura, R.S., Srivastava, S., Sharma, V., Sharma, P.K., Lal, C., Singh, M., et al., 2016. Role of interlayer spacing and functional group on the hydrogen storage properties of graphene oxide and reduced graphene oxide. Int. J. Hydrog. Energy 41, 9454–9461.
Rathnayake, R.M.N.M., Wijayasinghe, H.W.M.A.C., Pitawala, H.M.T.G.A., Yoshimura, M., Huang, H.H., 2017. Synthesis of graphene oxide and reduced graphene oxide by needle platy natural vein graphite. Appl. Surf. Sci. 393, 309–315.
Sakai, N., Yamamoto, S., Matsui, Y., Khan, M.F., Latif, M.T., Mohd, M.A., et al., 2017. Characterization and source profiling of volatile organic compounds in indoor air of private residences in Selangor State, Malaysia. Sci. Total Environ. 586, 1279–1286.
Sui, Z.Y., Meng, Q.H., Li, J.T., Zhu, J.H., Cui, Y., Han, B.H., 2014. High surface area porous carbons produced by steam activation of graphene aerogels. J. Mater. Chem. A 2, 9891–9898.
Wang, J., Chen, Z.M., Chen, B.L., 2014. Adsorption of polycyclic aromatic hydrocarbons by graphene and graphene oxide nanosheets. Environ. Sci. Technol. 48, 4817–4825.
Wang, X.B., Qin, Y.L., Zhu, L.H., Tang, H.Q., 2015. Nitrogen-doped reduced graphene oxide as a bifunctional material for removing bisphenols: synergistic effect between adsorption and catalysis. Environ. Sci. Technol. 49, 6855–6864.
Wang, H., Yang, W., Tian, P.H., Zhou, J., Tang, R., Wu, S.J., 2017. A highly active and anti-coking Pd–Pt/SiO_2 catalyst for catalytic combustion of toluene at low temperature. Appl. Catal. A 529, 60–67.
Yi, F.Y., Lin, X.D., Chen, S.X., Wei, X.Q., 2009. Adsorption of VOC on modified activated carbon fiber. J. Porous. Mater. 16, 521–526.
Yu, S.J., Wang, X.X., Ai, Y.J., Tan, X.L., Hayat, T., Hu, W.P., et al., 2016. Experimental and theoretical studies on competitive adsorption of aromatic compounds on reduced graphene oxides. J. Mater. Chem. A 4, 5654–5662.
Zhao, J., Wang, Z.Y., Zhao, Q., Xing, B.S., 2014. Adsorption of phenanthrene on multilayer graphene as affected by surfactant and exfoliation. Environ. Sci. Technol. 48, 331–339.